Tormann, T., Wiemer, S., Metzger, S., Michael, A., Hardebeck, J. L. (2013): Size distribution of Parkfield's microearthquakes reflects changes in surface creep rate. - Geophysical Journal International, 193, 3, pp. 1474—1478.

DOI: http://doi.org/10.1093/gji/ggt093

Geophysical Journal International

Geophys. J. Int. (2013) **193,** 1474–1478
Advance Access publication 2013 March 28

doi: 10.1093/gji/ggt093

EXPRESS LETTER

Size distribution of Parkfield's microearthquakes reflects changes in surface creep rate

T. Tormann,[1] S. Wiemer,[1] S. Metzger,[1,2] A. Michael[3] and J. L. Hardebeck[3]

[1] *Swiss Seismological Service, ETH Zurich, Switzerland. E-mail: thessa@sed.ethz.ch*
[2] *Helmholz Centre Potsdam, GFZ Potsdam, Germany*
[3] *U.S. Geological Survey, Menlo Park, USA*

Accepted 2013 March 5. Received 2013 February 27; in original form 2012 December 14

SUMMARY

The nucleation area of the series of *M*6 events in Parkfield has been shown to be characterized by low *b*-values throughout the seismic cycle. Since low *b*-values represent high differential stresses, the asperity structure seems to be always stably stressed and even unaffected by the latest main shock in 2004. However, because fault loading rates and applied shear stress vary with time, some degree of temporal variability of the *b*-value within stable blocks is to be expected. We discuss in this study adequate techniques and uncertainty treatment for a detailed analysis of the temporal evolution of *b*-values. We show that the derived signal for the Parkfield asperity correlates with changes in surface creep, suggesting a sensitive time resolution of the *b*-value stress meter, and confirming near-critical loading conditions within the Parkfield asperity.

Key words: Time-series analysis; Earthquake interaction, forecasting, and prediction; Seismicity and tectonics; Statistical seismology.

GJI Seismology

1 INTRODUCTION

The size distribution of earthquakes—described by the *b*-value from the Gutenberg & Richter (1944) law: log(Number of events with magnitude $\geq M$) $= a - bM$—has been shown to be inversely proportional to differential stresses: from acoustic emissions during fracture experiments in the laboratory (e.g. Amitrano 2003) to natural earthquakes in the crust (Schorlemmer & Wiemer 2005; Spada *et al.* 2013); the higher the differential stresses, the lower the *b*-values. *b*-Values have therefore been suggested to act as a crude stress meter for the crust, allowing us to image relative stress distributions, highlighting, for example, along faults areas of anomalous low *b*-values, that is, high stresses, so-called asperities, which are likely to emanate future larger ruptures (e.g. Wiemer & Wyss 1997). One well-studied example is the spatial distribution of *b*-values in Parkfield: a segment of the San Andreas Fault in central California, which is known for its series of six $M \sim 6$ events occurring relatively regularly over the last 150 yr (Bakun & Lindh 1985), and which is widely regarded among seismologists to be an ideal natural laboratory for improving our understanding of the earthquake cycle, the identification of main shock precursors and the development and testing of prediction models (e.g. Bakun *et al.* 2005). For this reason, back in the 1980s, dense and high-quality networks of monitoring instruments from various fields of Earth sciences were installed at the site of the 'Parkfield Experiment' (Bakun & Lindh 1985) to capture a wide range of geophysical signals of the approaching event and reveal possible precursors. Thus, the most recent Parkfield main shock was extremely well recorded, when it occurred in 2004, much later than expected. Despite the wealth of data, no unambiguous precursors were observed (Bakun *et al.* 2005). However, a low *b*-value anomaly in the nucleation area of the moderate main shocks had been documented before the latest event (Wiemer & Wyss 1997; Schorlemmer *et al.* 2004); and this structure reflects the approximate extent of the slip and aftershock distribution of the 2004 event, that is, it successfully 'postcasted' the location of the *M*6 event (Schorlemmer & Wiemer 2005). Tormann *et al.* (2012) re-evaluated the data for the pre- and postmain shock phases and found the asperity to be a stably stressed volume through the seismic cycle: shape and amplitude of the low *b*-value volume remains the same after the 2004 main shock. Fig. 1(a) shows the spatial *b*-value distribution derived from the last three decades of seismicity. A first-order time-series analysis of the asperity *b*-values showed that the 2004 event has not imprinted on the *b*-values beyond the first few months of aftershocks. The overall levels before and after the main shock are unchanged and, if converted into expected recurrence times of the *M*6 events, they are consistent with the observed interevent times.

In this study, we discuss techniques and uncertainties in detailed temporal *b*-value analysis and focus on second-order effects of the Parkfield time-series, namely the variation that is seen over the two decades before the main shock. This could be regarded as random fluctuation around a mean value, was it not for a data set of surface creep measurements from atop the asperity volume: the changes in creep rate correlate strongly with the signal seen in the *b*-value time-series and suggest that the state of stress at the fault at seismogenic depths is related to aseismic creep seen on the surface.

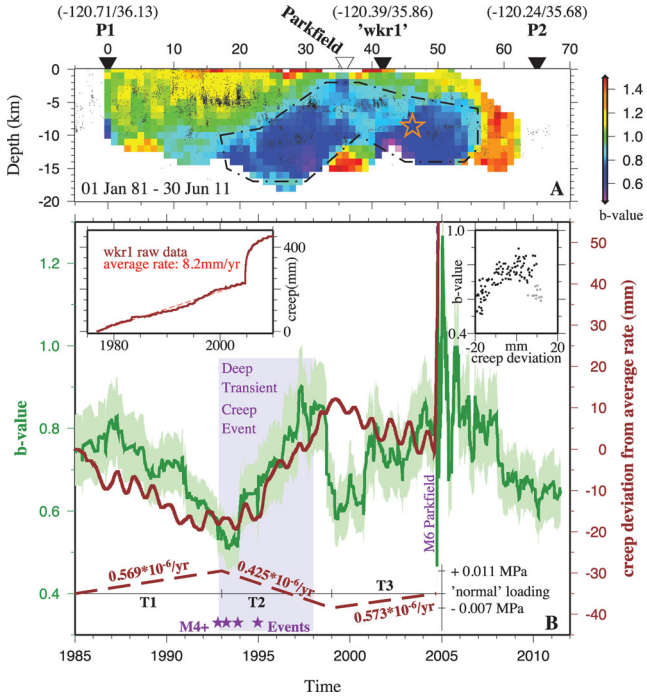

Figure 1. (a) *b*-Value cross-section for Parkfield's microseismicity $M \geq 1.3$ since 1981; star: 2004 *M*6 hypocentre; line: follows the $b = 0.87$ contour surrounding the asperity volume as defined in Tormann *et al.* (2012). (b) *b*-value time-series of asperity volume; Inset left: raw creep data collected from 'wkr1'; Mainframe: green: *b*-value evolution with standard error estimate (Shi & Bolt 1982), brown: deviation of creep from the average rate, that is, in 1993 the observed displacement on the instrument is ∼20 mm 'behind' the expected displacement, in 2000 it is ∼10 mm 'ahead', dashed brown line: from creep and therewith strain rate derived changes in loading relative to the expected normal loading based on the average creep rate of 8.2 mm yr^{-1}, purple shading: time period of a deep transient creep event in the asperity (Gao *et al.* 2000), accompanied by four *M*4–5 earthquakes (purple stars); Inset right: correlation plot of *b*-value time-series versus creep rate changes, sampled on a monthly basis, grey: data sampled during period of influence of the 5-d cluster.

2 THE *B*-CREEP CORRELATION OBSERVATION

Among the Parkfield monitoring instruments is the Work Ranch creepmeter ('wkr1'), which is located atop the centre of the asperity that produces the regular moderate earthquakes (Fig. 1a). Creep data on that instrument has been collected since 1976 (Fig. 1b, left-side inset), and as most creepmeters, 'wkr1' observes small-scale seasonal changes, but is regarded largely unaltered by rainfall events, and is mostly driven by tectonic signals (Roeloffs 2001). We remove the average creep rate of 8.2 mm yr^{-1} (1980 to before the 2004 event), and find a pattern of alternating decelerated and accelerated creep velocity phases over the two decades prior to the latest main shock (Fig. 1b). The average annual creep rate between 1985 and 1993 is with 6.1 mm yr^{-1} only ∼75 per cent of long-term average, during the following 6 yr it accelerates to 12.9 mm yr^{-1}, more than twice the previous velocity, and nearly 160 per cent of the long-term average, and after 1999 it slows down again to 5.9 mm yr^{-1}.

We calculate the time-series of *b*-values from within the low-*b*-value asperity volume (see Section 3 for the discussion of the method) and observe two separate properties of the temporal evolution (Fig. 1b): (1) As documented in Tormann *et al.* (2012), the first-order observation is a constant level of *b* for the pre- and post-main shock phases, with only a brief increase from the aftershock sequence. (2) Beyond that, we resolve second-order changes around the mean *b*-value, exceeding ±30 per cent over the last three decades: we observe three alternating ∼6 yr phases of decreasing, increasing and again decreasing *b*-values, before we measure very briefly, but sharply increased values (reaching $b > 1$) in the direct aftermath of the *M*6 event and decreasing *b*-values since then (Fig. 1b). The period of increasing *b*-values starting in 1993, coincides with the onset of a documented transient slip event in the asperity volume (Gao *et al.* 2000; Murray & Segall 2005), which was possibly initiated, but at least accompanied by a series of four *M*4–5 earthquakes and an increased seismicity rate of about 30 per cent above the average 1981–2004 rate. We observe a sudden deviation from the overall trends for a ∼2-yr period around 2000, when the *b*-values drop sharply. Much of this signal is produced by a 5-d cluster in mid-September 1998, rupturing within a 3 × 1.6 km fault patch located at 8 km depth. The eight $M \geq 1.3$ events have a mean magnitude of 2.4, while the asperity events following that cluster and through to the end of the 'anomaly' have a mean magnitude of 1.9, that is, all *b*-value estimates from time frames including this cluster (1998.75–2000.8) are decreased.

Comparing the two data sets we find that, with the exception of that short cluster-dominated period, the trends in the creep rate until 2004 are robustly correlated with the evolution of the *b*-value measured by the microseismicity right beneath the creepmeter (Fig. 1b and right-side inset). Decreasing *b*-values correlate with less surface creep, and vice versa. The observed changes in surface creep are therewith related to the (unknown) state of stress and strain at the fault at seismogenic depth. However, for the years after the 2004 main shock, the creep signal is strongly dominated by shallow afterslip (Barbot *et al.* 2009) that likely masks the deeper processes, which our *b*-values represent; we therefore do not compare the post-main shock data directly, but note that, overall, the annual creep rates since the main shock are decelerating non-linearly and contemporaneously the *b*-values are decreasing. Sudden changes in *b*-values, such as the drop in 1998 or the peak in 2004 are due to active clusters, which are to be expected in most studies given that seismicity clusters, and need to be treated individually and interpreted separately from long-term trends.

To develop an idea of the order of stress changes that Parkfield's *b*-values reflect, we use the different creep rates of 6.1, 12.9 and 5.9 mm yr^{-1}, as observed during time periods T1, T2 and T3 (Fig. 1b) to model the shear strain across that slowly creeping section of the fault and calculate the accumulated shear stress, that is, faster creeping reduces the strain/stress accumulation rate, and vice versa. We assume a relative plate motion of 33 mm yr^{-1} across the San Andreas Fault (Murray & Langbein 2006) and, for the sake of simplicity, we describe each fault creep variation with a uniform, rectangular dislocation in an elastic half-space (Savage & Burford 1973). The model segment extends from the surface down to 15 km depth (Murray & Langbein 2006) and is 20 times longer than the real Parkfield section to eliminate edge effects. The modelled maximum shear strain rates $\dot{\epsilon}_s$ across the central part of the model segment are then transformed into shear stress rates $\dot{\sigma}_s$ using the relationship $\dot{\sigma}_s = \mu\dot{\epsilon}_s$ that connects stress and strain with the shear modulus $\mu =$ 30 GPa (Murray & Segall 2005). Integrated over the different time periods T1–T3, the shear stress reveals the overall stress accumulation. These numbers are then compared to the 'expected' stress accumulation of the average creep rate, as measured until the 2004 Parkfield earthquake (8.2 mm yr^{-1}). Due to the lower than average creep rates in T1, we find an additional stress build up at the end of T1 of 0.011 MPa above the 'normal loading' from long-term creep

velocities, while at the end of T2, the stress build up is 0.007 MPa below the expected value (Fig. 1b). This variation is about an order of magnitude above the level of tide induced stresses (10^3 Pa, Tanaka *et al.* 2006), and tiny compared to the estimated absolute stress levels along the fault, which range from about 20 MPa in the weak fault hypothesis up to 160 MPa in the strong fault hypothesis (e.g. Scholz 2000).

We note that the above observation represents the data of only one creepmeter; but the two closest instruments next to 'wkr1' ('xta1' and 'crr1') have been reported for similarly accelerated velocities between 1993 and 1999 compared to their long-term trends (Roeloffs 2001). While our calculated amplitudes of stress variation probably reflect the specifics of the 'wkr1' instrument, the overall finding of correlating *b*-value and creep rate changes seems to be a more general pattern for the Parkfield asperity.

3 *b*-VALUE TIME-SERIES ANALYSIS: HOW TO RESOLVE DETAILS RELIABLY

Detailed temporal variation in *b*-values, such as shown in Fig. 1(b) can only be meaningfully documented and interpreted if the data and analysis techniques have been carefully chosen. In general, temporal variations of *b*-values are more difficult to identify than spatial variations (Wiemer *et al.* 1998); they are often of lower amplitude than their spatial counterparts and easily mimicked or masked by inhomogeneities in the catalogue or by the combination of spatial variability and changes in activity rate. To reliably analyse maximum likelihood *b*-values (Aki 1965) through time and establish the significance of potential changes the following issues need to be addressed:

(1) **Data quality: homogeneity of reporting**

Inhomogeneities of earthquake reporting are common in all earthquake catalogues and are an obstacle for a number of statistical analyses. Especially for interpreting *b*-values, it is important to use high quality and consistent earthquake catalogues, because changes in the monitoring network and processing inhomogeneity with time can introduce shifts and stretches in the magnitude scales which can mimic or mask changes in *b*-values (e.g. Zuniga & Wiemer 1999; Tormann *et al.* 2010).

The Parkfield segment of the San Andreas Fault is one of the best monitored fault segments in the world, and different high-quality data sets are available online. Schorlemmer *et al.* (2004) have shown that the spatial *b*-value distribution is consistent between the different data sets, that is, the ANSS and HRSN catalogues. We use the ANSS catalogue between 1981 January 1 and 2011 June 30 and verify that the introduction of the new M_L scaling in 2009 May, other than in southern California, did not alter the statistics of the local microseismicity magnitude range (Tormann *et al.* 2010).

(2) M_c **variability**

The correct assessment of the completeness magnitude, M_c, of an earthquake sample is critical for the correct estimate of the *b*-value: if M_c is underestimated, *b*-values will be systematically biased towards too low values. Especially, important for temporal *b*-value analysis is the verification of the completeness level through time, for example, M_c usually decreases when the network is improved and new instruments are added, and it often increases temporarily after large earthquakes (e.g. Woessner & Wiemer 2005).

For the Parkfield asperity, we assess M_c using the maximum curvature estimate and adding 0.2 for safety. We confirm a reasonable estimate of $M_c = 1.3$, as published by Schorlemmer *et al.* (2004). We verify that the overall shape of the time-series does not change for at least $1.1 \leq M_c \leq 1.8$.

(3) **Spatially homogeneous volume**

In the presence of spatially heterogeneous *b*-values, local changes in activity rate can cause apparent changes in *b* through time (e.g. Wiemer *et al.* 1998). It is important, before interpreting changes in temporal *b*-value evolution, to verify that they are not unintended artefacts from emphasizing different spatially distinct volumes that are seismically active during different periods, instead of true temporal changes in the behaviour within the same volume. The temporal analysis, therefore, needs to be restricted to a volume that is spatially homogeneous. To identify potential regions, Wiemer *et al.* (1998) have proposed the technique of differential *b*-value mapping, in which they calculate *b*-value grids for two subsequent time periods and map the percentual difference for all nodes that have a *b*-value estimate in both periods, and show a difference in these estimates beyond a certain statistical significance level. This technique highlights areas of significantly increased or decreased *b*-values, but is in its resolution and spatial coverage highly dependent on and limited to the choice of time periods. It is an effective approach if the approximate time of a potential change is known or suspected beforehand, for example, an independent geodetic observation or a large close or distant main shock; it is less suitable for an 'uninformed' analysis of temporal *b*-value evolution.

We introduce a Spatial HOmogeneity Detecting technique (SHOD), which evaluates for a given volume the spatial homogeneity through time by combining spatial and temporal analysis of *b*-values: we first map the spatial distribution of *b*-values to select the volume for the temporal analysis and assign each earthquake in the sample volume the closest *b*-value from the spatial mapping. At each time step, we calculate the *b*-value from the current time window of the sample and, in addition, the mean of the associated spatial *b*-values from the events of that time frame. If that spatial curve follows the curve of the time-series, the temporal signal is artificial and produced by sampling different subvolumes at different times, that is, the underlying earthquake sample was spatially inhomogeneous. For a homogeneous volume, the spatial curve will be more or less flat. Figs 2(a) and (b) show this effect for a synthetic catalogue, and (c) verifies that the spatial curve for the Parkfield asperity volume (Fig. 1a, all earthquakes inside the $b = 0.87$ contour) is well behaved.

(4) **Constant-time-windows or fixed-number-of-events approach?**

Temporal *b*-value studies often use fixed length time windows to estimate *b*-values through time. We argue that this approach has severe disadvantages in a time-series of significantly varying activity rates: one can either use small time windows and be able to track immediate changes, for example, due to a main shock and its early aftershocks, but then create many empty time bins in less active parts of the series; or else one keeps the windows long enough to fill every bin, but then lose the detailed information on any abrupt changes and create an apparent shift due to considering 'too old' data/processes in each estimate (Fig. 3). The alternative is to instead use moving windows of a fixed number of *N* events. The choice of *N* is subjective and determines the level of uncertainty in each *b*-value estimate (higher for smaller *N*), and the degree of smoothing/damping of signals (stronger for larger *N*). This fixed *N* technique provides an estimate at each point in time, which represent data from different lengths of time windows, though: from a few days or weeks during an active aftershock sequence to several years in seismically quiet periods.

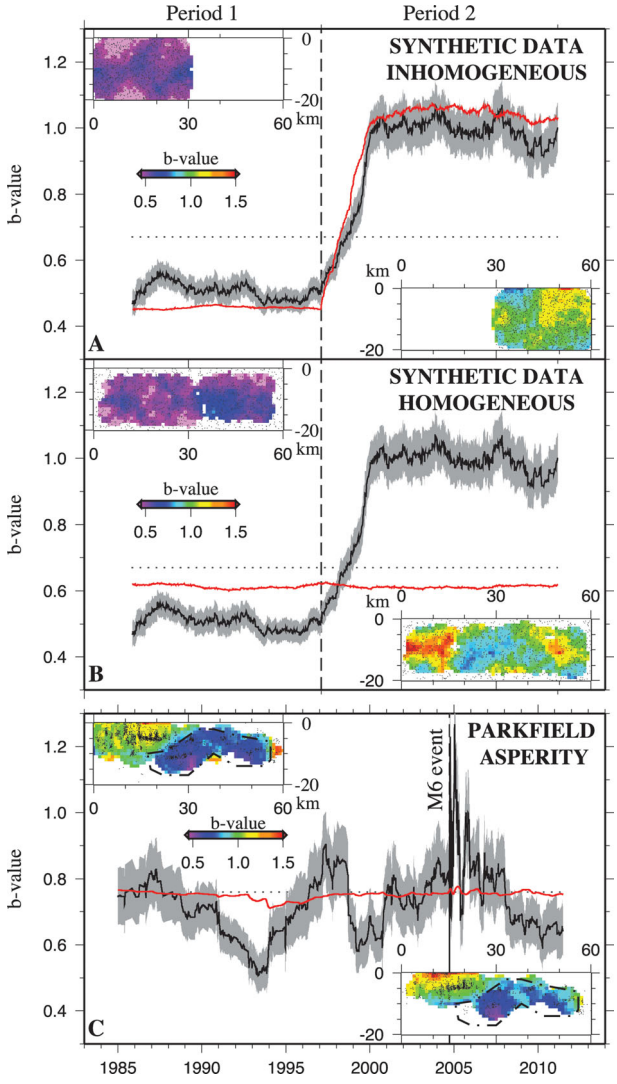

Figure 2. SHOD: spatial homogeneity detector for temporal *b*-value analysis. (a and b) Synthetic example of a spatially (a) inhomogeneous volume (two distinct regions of different *b*-values and activation periods, 0–30 km during period 1 and 30–60 km during period 2), and a (b) homogeneous volume (evenly distributed events throughout the full volume), both with $b = 0.5$ in period 1 and $b = 1$ in period 2. Black/grey: *b*-value time-series and formal uncertainty, red: mean of closest spatial *b*-values, dotted line: overall mean *b*-value of the volume. Cross-sections: spatial *b*-value distributions for time periods 1 and 2. (c) Analysis applied to Parkfield data, cross-sections cover before and after the 2004 main shock, flat red curve confirms spatial homogeneity, so temporal variations in the black data are not artefacts.

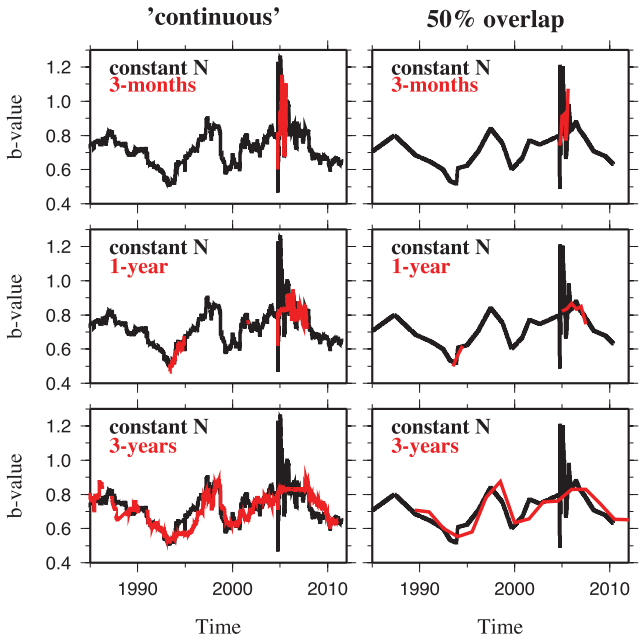

Figure 3. Comparison of *b*-value time-series for different sampling techniques: constant number, *N*, of events (black) versus constant time, *T*, windows (red): always $N = 68$, *T* increases from 3 months to 3 yr (top to bottom); left-hand panels show continuous sampling for either of the combinations, that is, windows are moved by one-event or 1-d steps, respectively; right-hand panels show the same combinations for 50 per cent overlap sampling: windows are moved by half their length, that is 34 events or 1.5 months, 0.5 and 1.5 yr, respectively. The gaps in the *T* curves represent times of too little activity to calculate *b*-values, the 3-yr sampling does not capture the abrupt change due to the 2004 main shock.

We use the average annual number of events within the Parkfield asperity between 1981 and 2011, $\overline{N}_{\text{ann}} = 68$, which results in individual window lengths averaging around 3 yr. We demonstrate the differences between the alternative approaches for window sizes of 3 months–3 yr compared to $\overline{N}_{\text{ann}}$-event sampling (Fig. 3). Apart from the explained limits of the constant time window sampling, the choice of either that or the constant number approach does not matter for the shape of the curve. We verified that changing the value of *N* within reasonable limits (e.g. $50 \leq N \leq 150$) also preserves the general shape of the time-series.

(5) **Step sizes**

A further free parameter is the overlap between successive *b*-value estimates in the time-series, which is a trade-off between smoothing and number of data points together with the independence of the starting point. The smaller the overlap, that is, the larger the step size relative to the window length, the larger the sensitivity to the 'gridding', that is, the starting time or event.

We prefer the continuous approach of moving the window by one event at a time, and note that the overall shape is retrieved with any step size, from continuous to no overlap (Fig. 3).

(6) **Data display**

b-Values from temporal analysis are either plotted at the beginning, middle or end of the time window that they represent. We argue that the latter choice is the most sensible to physically understand the resolved signals of the time evolution, since it represents the *b*-values as result of previous seismicity, that is, changes that are caused by a large event with its immediate aftershocks will plot at/after their actual occurrence, not before, as would happen for either of the alternative display modes and be confusing for interpretation. We note that with this choice, the Parkfield time-series starts in 1985 although it uses all events since 1981 (Fig. 1b).

(7) **Significance check**

Each of the above factors influences the shape of the *b*-value time-series and adds uncertainty to the formal standard deviation (Shi & Bolt 1982) of the estimated *b*-value, which is mostly driven by the number of events in the earthquake sample. Any temporal *b*-value study interested in details of the time-series needs to carefully address the above points and establish that the interpreted signals are meaningful beyond uncertain fluctuation. We evaluate the sensitivity of our results to the choice of all these free parameters within sensible ranges, and find the major structures to be common for all choices, confirming the robustness of the signal.

4 DISCUSSION AND CONCLUSION

The observation of a correlation between seismic and geodetic transients, shown here, is at least the second of its kind: from Japanese data, Wiemer *et al.* (2005) documented a correlation between an increase in *b*-values in the Tokai region and a contemporaneously accelerated subsidence rate.

The temporal correlation between *b*-value transients and creep data is fully consistent with a model where the size distribution of the microseismicity responds to changes in the stressing regime. When creep slows down and loading stresses on the fault increase, little rough patches on the fault tend to break not one by one, but in groups, creating more often larger microearthquakes, decreasing the *b*-value, implying higher probabilities for larger magnitude earthquakes. In times of accelerating creep, stresses are released to a higher degree aseismically, tiny rough patches on the fault can break on their own, without jumping to neighbouring patches, the magnitudes of the microseismicity are preferably small, the *b*-values high. The suggestion is that *b*-values thus can act as a stress meter not only in a spatial sense but also have the temporal resolution to track loading levels through time.

Stress perturbations caused by tides are relatively small; this led Tanaka *et al.* (2006) to argue that local stress conditions must be close to a critical state for tidal stresses to trigger earthquakes. In a systematic study of tidal triggered earthquakes they could identify strong correlations of small magnitude earthquake occurrence rates and tidal stress changes in focal regions prior to major earthquakes, but lost the signal after the main ruptures (i.e. significant stress releases). Based on their conclusions, the Parkfield *b*-creep correlation observation is plausible, if the stress state is near critical such that there is always the possibility of moderate events (Tormann *et al.* 2012). Then, the distribution of event sizes can be modulated by small changes in the stress state. This differs from previous results in which *b*-values were thought to only react to drastic changes in the environment (Wiemer *et al.* 1998).

The small-scale fluctuations are apparently also not the driving factor in the timing of a major event, since the 2004 main shock did not occur at a *b*-value minimum. The triggering mechanism for the *M*6 type events remains unknown for the time being.

Our results suggest that monitoring *b*-values through time can resolve major changes in local stress fields as previously documented in a volcanic environment for a magma intrusion (Wiemer *et al.* 1998) and along-fault for the Loma Prieta *M*7 earthquake (Tormann *et al.* 2012), and has the potential to indicate near-critically stressed structures. This is particularly valuable, since the mere comparison of absolute *b*-values does not allow a direct translation into stress levels, they only represent relative stress distributions. By estimating the strain-sensitivity of *b*-value time-series using geodetic data, an improved assessment of the current loading stage of hazardous asperities may become possible.

ACKNOWLEDGEMENTS

We thank J. Rubinstein, A. Llenos and an anonymous reviewer for helpful comments. Earthquake data were obtained from http://www.ncedc.org/anss/catalog-search.html (last accessed 19 March 2013) and creepmeter data from John Langbein's database at ftp://ehzftp.wr.usgs.gov/langbein/CREEP/ (last accessed 19 March 2013). Figures were produced with the generic mapping tools [http://gmt.soest.hawaii.edu/ (last accessed 19 March 2013)]. Part of this study was funded through SNF grant PMPDP2 134174.

REFERENCES

Aki, K., 1965. Maximum likelihood estimate of b in the formula $\log N = a - bM$ and its confidence limits, *Bull. Earthq. Res. Inst.,* **43,** 237–239.

Amitrano, D., 2003. Brittle-ductile Ttransition and associated seismicity: experimental and numerical studies and relationship with the *b* value, *J. geophys. Res.,* **108**(B1), doi:10.1029/2001JB000680.

Bakun, W.H. & Lindh, A.G., 1985. The Parkfield, California, earthquake prediction experiment, *Science,* **229,** 619–624.

Bakun, W.H. *et al.*, 2005. Implications for prediction and hazard assessment from the 2004 Parkfield earthquake, *Nature,* **437,** 969–974.

Barbot, S., Fialko, Y. & Bock, Y., 2009. Postseismic deformation due to the *M*w 6.0 2004 Parkfield earthquake: stress-driven creep on a fault with spatially variable rate-and-state friction parameters, *J. geophys. Res.,* **114**(B7), doi:10.1029/2008JB005748.

Gao, S., Silver, P.G. & Linde, A.T., 2000. Analysis of deformation data at Parkfield, California: detection of a long-term strain transient, *J. geophys. Res.,* **105,** 2955–2967.

Gutenberg, B. & Richter, C.F., 1944. Frequency of earthquakes in California, *Bull. seism. Soc. Am.,* **34,** 185–188.

Murray, J.R. & Langbein, J., 2006. Slip on the San Andreas Fault at Parkfield, California, over two earthquake cycles, and the implications for seismic hazard, *Bull. seism. Soc. Am.,* **96**(4B), S283–S303.

Murray, J.R. & Segall, P., 2005. Spatiotemporal evolution of a transient slip event on the San Andreas Fault near Parkfield, California, *J. geophys. Res.,* **110**(B9), doi: 10.1029/2005JB003651.

Roeloffs, E., 2001. Creep rate changes at Parkfield, California 1966–1999: seasonal, precipitation induced, and tectonic, *J. geophys. Res.,* **106,** 16525–16547.

Savage, J.C. & Burford, R.O., 1973. Geodetic determination of relative plate motion in central California, *J. geophys. Res.,* **78,** 832–845.

Scholz, C.H., 2000. Evidence for a strong San Andreas Fault, *Geology,* **28**(2), 163–166.

Schorlemmer, D. & Wiemer, S., 2005. Earth science: microseismicity data forecasts rupture area, *Nature,* **434,** doi:10.1038/4341086a.

Schorlemmer, D., Wiemer, S. & Wyss, M., 2004. Earthquake statistics at Parkfield: 1. Stationarity of *b* Values, *J. geophys. Res.,* **109**(B12), doi:10.1029/2004JB003234.

Shi, Y. & Bolt, B.A., 1982. The standard error of the magnitude-frequency *b* value, *Bull. seism. Soc. Am.,* **72,** 1677–1687.

Spada, M., Tormann, T., Wiemer, S. & Enescu, B., 2013. Generic dependence of the frequency-size distribution of earthquakes on depth and its relation to the strength profile of the crust, *Geophys. Res. Lett.,* **40,** in press.

Tanaka, S., Sato, H., Matsumura, S. & Ohtake, M., 2006. Tidal triggering of earthquakes in the subducting Philippine Sea Plate beneath the locked zone of the plate interface in the Tokai Region, Japan, *Tectonophysics,* **417,** 69–80.

Tormann, T., Wiemer, S. & Hauksson, E., 2010. Changes of reporting rates in the Southern Californian Earthquake Catalog, introduced by a new definition of ML, *Bull. seism. Soc. Am.,* **100**(4), 1733–1742.

Tormann, T., Wiemer, S. & Hardebeck, J., 2012. Earthquake recurrence models fail when earthquakes fail to reset the stress field, *Geophys. Res. Lett.,* **39,** doi:10.1029/2012GL052913.

Wiemer, S. & Wyss, M., 1997. Mapping the frequency-magnitude distribution in asperities: an improved technique to calculate recurrence times? *J. geophys. Res.,* **102,** 15115–15128.

Wiemer, S., McNutt, S.R. & Wyss, M., 1998. Temporal and three-dimensional spatial analyses of the frequency-magnitude distribution near Long Valley Caldera, California, *Geophys. J. Int.,* **134,** 409–421.

Wiemer, S., Yoshida, A., Hosono, K., Noguchi, S. & Takayama, H., 2005. Correlating seismicity parameters and subsidence in the Tokai Region, Central Japan, *J. geophys. Res.,* **110**(B10), doi:10.1029/2003JB002732.

Woessner, J. & Wiemer, S., 2005. Assessing the quality of earthquake catalogues: estimating the magnitude of completeness and its uncertainty, *Bull. seism. Soc. Am.,* **95,** 684–698.

Zuniga, F.R. & Wiemer, S., 1999. Seismicity patterns: are they always related to natural causes? *Pure appl. Geophys.,* **155,** 713–726.